Memory characteristics studies for large deflections in amorphous polymers: Experiments and numerical simulation

R Sujithra, MS Srinivasan and A Arockiarajan

Abstract

In this work, the shape memory behaviour for large deflections in a ring-shaped epoxy-based shape memory polymer specimen is studied. A thermo-mechanical test setup was built to study the memory characteristics of ring shaped specimens with three different ratios of epoxy resin and hardener. Thermo-mechanical characterizations were also carried out to understand the material behaviour during shape fixing and recovery phases and also to obtain the material parameters for numerical simulations. Numerical simulations are carried out using a model proposed earlier by the authors based on the theory of multiple natural configurations and implemented using the VUMAT feature of ABAQUS commercial software. The simulation results for free shape recovery and constraint load recovery for large deflections confirm that the model performs well especially in relation to the memory dependent characteristics.

Keywords

Epoxy SMP, large deflections, memory characteristics, ABAQUS-VUMAT, multiple natural configurations

Introduction

Shape memory polymers (SMPs) are generally referred to as active materials having the capability to store any deformed temporary shape and regain the permanent shape by the application of a non-mechanical stimulus usually by heat (Lendlein and Kelch, 2002). SMPs are a low cost material that are light weight, have excellent large shape recovery, tailor made properties and are biodegradable. These features makes SMPs suitable for numerous applications such as space deployable and morphing structures (Liu et al., 2014), biomaterials (Lendlein and Behl, 2008; Yakacki et al., 2007), smart textiles, automobile actuators and self-healing composite systems (Li, 2014). Since its applications are diverse in all the emerging fields, there is a need for triggering the shape recovery by other stimuli such as an electric field (Leng et al., 2007), magnetic field (Mohr et al., 2006), laser (Maitland et al., 2002) and or solution (Lv et al., 2008). This indirect stimulus is achieved by adding fillers or by stimuli sensitive groups at the molecular level (Behl and Lendlein, 2007). For example in electro-active SMPs, carbon nanoparticles or conductive fibres are introduced into the SMP matrix to improve the electrical properties (Liu et al., 2009). Similarly, to enhance high strength and high stress

recovery in SMPs, the fibre is reinforced into the SMP matrix without compromising shape recovery characteristics (Lan et al., 2009). In addition, SMPs are not only limited to dual shape memory effect, but also triple shape memory effect with two reversible phases (Zotzmann et al., 2010) or a multi-shape memory effect with a single broad transition temperature (Xie, 2010). This shows that the shape memory effect in polymers is a combination of molecular architecture together with the programming technique. Extensive reviews on SMP stimulus methods, functionality with applications are described by Leng et al. (2011) and Meng and Li (2013).

The SMP network consists of netpoints or hard segments and the switching domain or reversible phase. SMPs are classified based on the transition temperature of the cross-links (physical or chemical) and by the switching domains. A detailed description of SMP

Department of Applied Mechanics, Indian Institute of Technology Madras, Chennai, India

Corresponding author:
A Arockiarajan, Department of Applied Mechanics, Indian Institute of Technology Madras, 600036 Chennai, India.
Email: aarajan@iitm.ac.in

Downloaded from jim.sagepub.com at RYERSON UNIV on June 17, 2015

structures, classification, shape memory cycle mechanism, functionality and applications is reviewed by Hu et al. (2012). Among these classifications, the simplest type of SMP is the amorphous cross-linked thermoset glassy polymer with a single glass transition temperature. Also, this amorphous cross-link thermoset glassy polymer is reported to have excellent shape recovery characteristics and no molecular slippage occurs between the chains due to chemical cross-linking (Liu et al., 2007; Rousseau, 2008). Hence, in the present work, chemically cross-linked epoxy-based SMP is chosen to characterize the shape memory behaviour of amorphous polymers.

In the chemically cross-linked polymer network, the polymer chains are connected by the netpoints. Above the transition temperature, the polymer chains are randomly coiled between the netpoints. When the SMP is deformed to a temporary shape, the polymer chains in the permanent network are elongated in the direction of stretch and thereby reducing the entropy of the system. By cooling below transition temperature, the elongated polymer chains form temporary cross-links with the side chains or chain segments due to an increase in intermolecular interactions or decrease in the molecular mobility. The deformed network is locked by the newly formed temporary cross-link of the polymer chains to store the temporary shape in the glassy state. Again by heating above the transition temperature, mobility of the chain segment increases and detached the temporary cross-links. Due to entropy elasticity, the chain segments are forced back to random coil configuration, resulting in permanent network or shape.

The shape memory properties of SMPs can be tailor-made by varying the chemical composition. The functionality of the cross-linker relates to the cross-link density (CLD) which in turn determines the glass transition temperature and also its structural properties (Garcia et al., 2007). Xie and Rousseau (2009) demonstrated the feasibility of tuning the epoxy-based SMPs by changing the glass transition temperature by varying the CLD or by replacing the rigid groups with flexible epoxy chains. Zhou et al. (2011) investigated the shape memory effect of epoxy-based SMPs in bending experiments by varying the flexibilizer content. Several epoxy-based SMPs have been designed for various purposes such as actuators (Leonardi et al., 2011), morphing applications (Tandom et al., 2009), high flexural strength (Rimdusit et al., 2013) and higher shape recovery ratio (Fan et al., 2013).

Apart from the molecular structure and composition, the response of the SMPs under complex force and temperature conditions aid in understanding the behaviour of the material for desired applications. Several studies on thermo-mechanical testing of SMPs have been reported in the literature as follows. The shape memory cycle experiments were performed for tension and compression in the small strain region (Liu et al., 2006), bending (Liu et al., 2003) and twisting (Diani et al., 2011) modes of deformations. It is reported that the performance of the material is also influenced by time- and temperature-dependent factors such as loading and unloading temperature, heating/cooling rate and rate of loading. Chen et al. (2014) studied the mechanical behaviour of epoxy SMP based on the effect of temperature and strain rate during loading at the vicinity of T_g. It is observed that during loading the stress levels exhibits strong strain rate and temperature sensitivity. Atli et al. (2009) conducted thermo-mechanical uniaxial tension test up to 75% strain by loading at temperatures above T_g (90 °C, 105 °C and 120 °C). Schmidt et al. (2008) studied the shape recovery properties under fatigue test (20 cycles). Fatigue experiments shows that during early cycles of loading, the amount of irreversible strain increases which saturates out after a certain number of cycles. Volk et al. (2010) conducted a series of tensile tests to study the free recovery behaviour by increasing the value of extension 10%, 25%, 50% and 100% strain. A shift in shape recovery was observed in their experiments, considering the rate effects which varied from 1 to 5 °C/min. Castro et al. (2011) investigated the amount of recovery strain and recovery rate under different thermal conditions. McClung et al. (2011) compared the free strain recovery measurements using contact (clip extensometer and strain gage) and non-contact (DIC and laser extensometer) methods. The shape memory performance was also investigated by varying the deformation rate, holding times and multiple thermo-mechanical cycles. A faster deformation rate and a small holding time in the rubbery region were recommended by the McClung et al. (2013) to enable better subsequent shape recovery. Rousseau and Xie (2010) reported that the shape memory performance is strongly influenced by the strain-dependent thermal expansion/contraction during shape memory cycle. Guo et al. (2014) investigated the influence of the applied stress on the phase transition temperature from creep experiments. In a typical shape memory cycle, shape fixing and recovery is usually done above or within the glass transition band. To simplify the shape fixing process, Li and Xu (2011) proposed cold compression thermoset programming below the transition temperature. The amount of pre-strain and stress relaxation time determines the shape fixity and recovery ratio in the cold compression programming.

In most of the applications, structures undergo complex shape changes which involve large deflections. For example in the design of multi-state components and smart bias components, Ghosh et al. (2013) proposed a design for smart valves using a SMP ring and a shape memory alloy (SMA) spring. In the present work, an attempt has been made to carry out the shape memory cycle experiments for large deflections using ring shaped specimen. A simple thermo-mechanical test setup was

Table I. Material characterization for various epoxy ratios.

Sample	Hardener ratio (phr)	E_r (MPa)	E_g (MPa)	T_g°C	Tanδ	E_g / E_r	E_r / E_g	Transition Width (°C)	CLD (mol/m^3)	CTE (1/°C) (Glassy state)
Epoxy85	7.673	10	1862	73	0.72	186.2	0.0054	31	1593	0.6×10^{-4}
Epoxy100	9.03	16	2140	86	0.59	133.7	0.0074	34	2697	0.48×10^{-4}
Epoxy115	10.38	20	2256	83	0.55	112.8	0.0089	28	3410	0.31×10^{-4}

built for measuring the shape fixing and recovery properties. The objective was to study the memory characteristics for large deflections in epoxy-based SMP, for different ratios and shape memory cycle parameters. Also, the shape memory cycle for this ring is numerically simulated in ABAQUS-VUMAT using the model based on the theory of multiple natural configurations proposed earlier by the authors (Sujithra et al., 2014). The material parameters used for the simulation are obtained from characterization experiments. The paper outline is as follows; in the following section we describe the materials chosen, experimental set-up and procedures followed for the memory cycles. Then we present the experimental results and discuss them in the light of shape storage and recovery behaviour. Finally the numerical simulations for the ring-shaped SMP specimens undergoing large deflections are presented and discussed.

Experiments

Epoxy sample preparation

The aromatic epoxy-based SMP is prepared using the commercially available phenolic modified diglycedyl ether of bisphenol A (EP-286FL) and triethyleneteramine (EH-758) as a hardener. Based on the epoxy curing chemistry, the desired stoichiometric quantity (Epoxy100) for curing is calculated as 9.03 parts of hardener per hundred parts of resin (phr). In addition, samples are also prepared at 15% deficient (Epoxy85) and 15% excess (Epoxy115) stoichiometries based on the hardener. The composition details of three different epoxy ratios that are prepared are given in Table 1. The monomer and hardener are hand mixed for 10 minutes to avoid air bubbles. The mixture is poured into a Teflon mould and covered with a plate to maintain uniform thickness as shown in Figure 1. The mould is cured at 60 °C for 2 hours and then post cured at 120 °C for 2 hours. The dimensions of the ring specimen with rectangular cross-section are as follows, outer diameter of 60 mm, inner diameter of 54 mm and thickness of 4.5 mm. After curing, the samples are demoulded and the edges are polished using silicon carbide paper.

Figure I. Teflon mould for a ring-shaped specimen.

Characterization

The DMA experiments are conducted in tensile mode using TA Instruments. The sample dimension used for the test is $50 \times 6 \times 0.4$ mm^3. The test is carried out in a multi-frequency strain mode at 1 Hz with a static force of 0.01 N. The mechanical response such as storage modulus, loss modulus and tanδ are obtained in the temperature range from 27 to 140 °C with a heating/cooling rate of 2 °C/min. The CLD is calculated from the volume fraction of the polymer when swollen in a methanol solvent. The detailed procedure for determining the CLD by swelling method is given by Sekkar et al. (2007). The thermal expansion of epoxy sample $(50 \times 12.5 \times 6$ mm$^3)$ is measured using the push rod-type dilatometer from 30 to 50 °C for glassy state.

Experimental setup and procedure for shape memory test

The experiments are carried out to study the shape memory behaviour for different epoxy ratios under various conditions in the following thermo-mechanical cycle (ABCD). A typical SMP cycle for ring shape is shown in Figure 2 and the process from (1) to (4) given below constitute the shape memory cycle.

1. Loading (deformation of permanent shape to temporary shape, A–B).
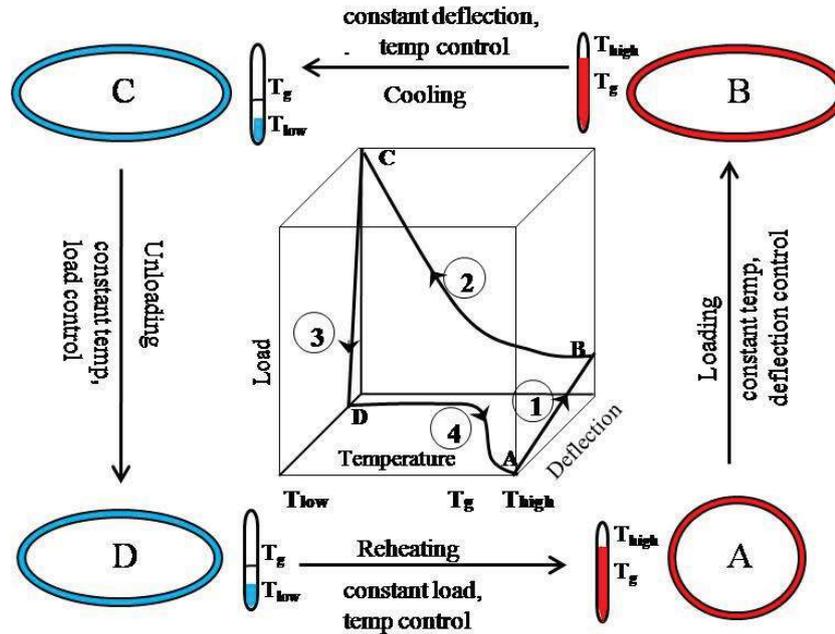2. Cooling (stores the temporary oval shape, B–C).

Figure 2. Schematic representation of SMP cycle.
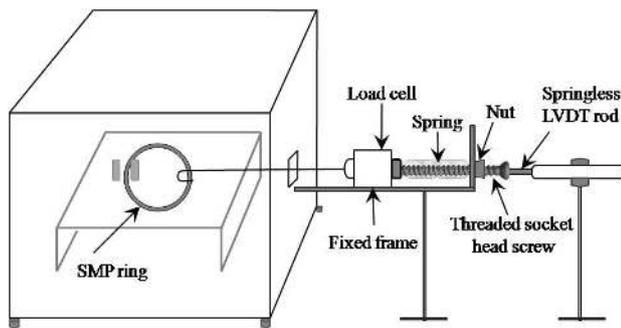

Figure 3. Schematic diagram of thermo-mechanical test setup for a SMP ring.

3. Unloading (temporary shape is retained with small spring back, C–D).
4. Reheating (free shape recovery, D–A).

The schematic diagram of experimental setup for a ring specimen is shown in Figure 3. At the beginning of the shape memory cycle, the SMP ring specimen is placed inside the chamber and the temperature in the chamber is brought to loading temperature (T_{load}) and maintained at T_{load} for 5 minutes. The chamber temperature was programmed using a PID controller unit and monitored using a thermocouple. The ring specimen is clamped at one side and hooked to thin wire at the other side. The thin wire is connected to the load cell to measure the force required for deforming the ring (permanent) to an oval (temporary) shape. The

threaded socket head screw is fixed to a load cell on one end and a springless LVDT rod is screwed on the other end. The threaded screw moves along the rotating nut giving a linear displacement due to which the load cell arrangement slides backward in the smooth fixed frame, which stretches the ring specimen. The amount of stretching is same as the displacement of the screw which is measured using the LVDT. The oval shape is held fixed in this position and the chamber is allowed to cool naturally (cooling rate is not uniform). By releasing the nut after cooling, the fixed temporary oval shape is unloaded. The load cell, LVDT and thermocouple values are recorded using Data Translation 9837 card. Finally, upon reheating to T_{high}, the stored oval shape changes to permanent circular shape. The LVDT is placed in front of the chamber slot to measure the shape recovery. The temperature and displacement of the free end of the sample are recorded for shape recovery. The photographs of the experimental set-up are shown in Figure 4(a) for shape fixing and Figure 4(b) for shape recovery.

Results and discussion

Three ratios of epoxy ring specimens are prepared for 15% deficient (epoxy85), 15% excess (epoxy115) and the stochiometric amount of hardener composition (epoxy100). The response of SMP material observed during the shape memory cycle experiments are discussed in this section.
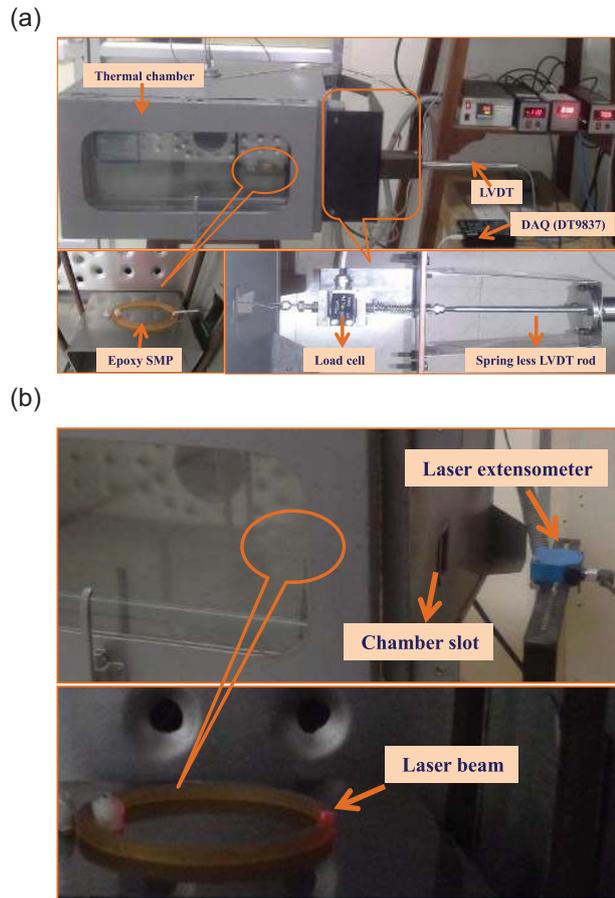
(a)

(b)

Figure 4. Photographs of a thermo-mechanical setup with a SMP ring sample.

Figure 5. DMA curve for different epoxy ratios.

Material characterization

Material characterization helps in determining the thermo-mechanical properties of SMPs. The results from DMA for different epoxy ratios are shown in Figure 5. The variation of stiffness with temperature and glass transition temperature is determined from the storage modulus and tanδ curve. In the storage modulus curve, a flat region for glassy (T_{low}) and rubbery (T_{high}) states is observed. The transition between these two states is referred as T_g band or transition region. The glassy stiffness (E_g) is of two orders of magnitude higher compared with the rubbery stiffness (E_r) for all of the epoxy ratios. The peak in the tanδ curve determines the glass transition temperature (T_g) and relates to the viscous nature of polymer. The material properties obtain from DMA and the cross-link densities obtained from swelling method are compared for all ratios in Table 1. By increasing the hardener ratio, the cross-linking density increases which renders an increase in the rubbery modulus. High CLD reduces the chain flexibility. The glass transition temperature can also be tuned based on the hardener ratio and relates to the mobility of the chain segments. The glassy
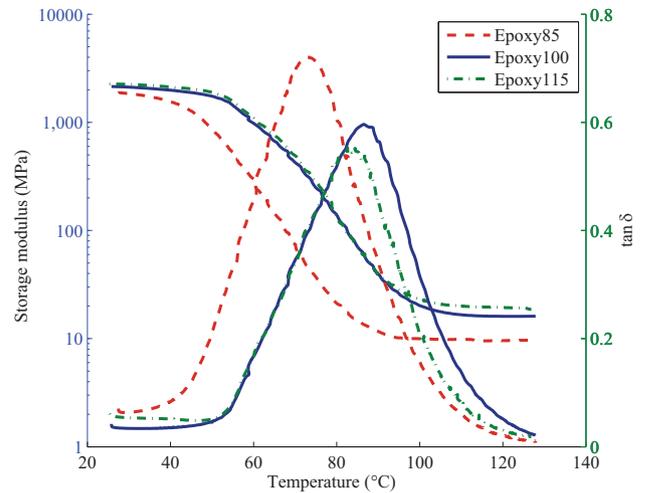
stiffness also increases by increasing the hardener ratio. It is observed that the decrease in the CLD, increases the amplitude of the tanδ peak due to increase in the chain flexibility.

It is reported in the literature that the shape memory cycle time will be shortened for materials with lower rubbery to glassy modulus (E_r / E_g) and higher tanδ peak (Rousseau and Xie, 2010). The high elasticity ratio (E_g / E_r) shows easy shaping at temperature above T_g and great resistance to deformation below T_g (Ratna and Kocsis, 2008). Lower rubbery to glassy modulus (E_r / E_g), higher tanδ and high elasticity ratio (E_g / E_r) are observed in epoxy85. The transition band also relates to the sensitivity of the material properties around T_g (Xie and Rousseau, 2009). The width of glass transition is measured from the width of tanδ peak at half height. An increase in CLD, shows the reduction in the transition band width. The epoxy115 has higher hardener content, but a relatively lower T_g and transition width compared with epoxy 100. Hence, the shape memory cycle time for epoxy115 will be smaller than epoxy100. An increase and decrease in the width of the tanδ peak indicates the material with lower (Epoxy85) and higher degrees (Epoxy115) of cross-linked network.

The results from the dilatometer tests for measuring thermal expansion in glassy state showed that the increase in CLD reduces the thermal expansion coefficient (Table 1). Apart from chemical composition, the thermo-mechanical experimental conditions are also expected to influence the shape memory behaviour which is discussed in the following sections.

Thermo-mechanical shape memory cycle test

The thermo-mechanical shape memory cycle experiments for three different epoxy ratios are carried out using the test setup as explained in previous section. The permanent shape ring is denoted by its diameter,
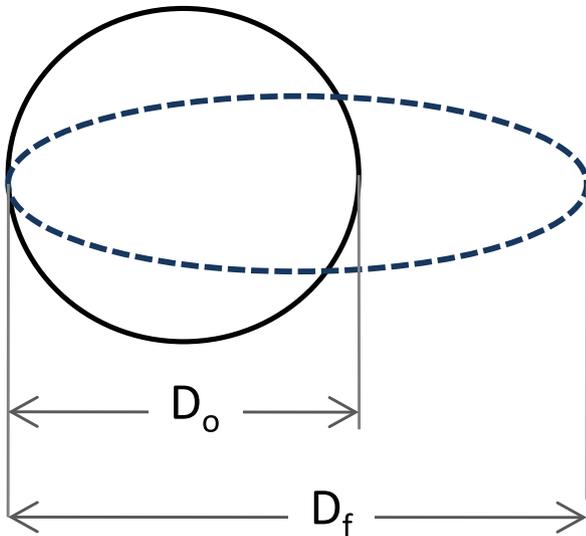
Figure 6. Ring shape SMP.

D_o (60 mm) and the deformed oval shape, represented as an ellipse, is denoted by its major principle axis diameter D_f as shown in Figure 6.

Shape memory cycle for different epoxy ratios

To study the shape memory behaviour for all of the epoxy ratios, the SMP ring is deformed diametrically by 15 mm ($D_f = 75$ mm) to an oval shape at a temperature of $T_g + 12$ °C (T_{load}). The specimen in the thermal chamber is heated to T_{load} at a rate of 3 °C/min and the temperature at T_{load} is maintained for 5 minutes. The ring-shaped specimen is deformed to oval shape ($D_f = 75$ mm) using a screw-type arrangement as the load required to pull the specimen is very low in the rubbery state. The isothermal loading curve (step 1, A–B) for three different epoxy ratios are represented by the non-linear behaviour in the force–deflection curve as shown in Figure 7(a). It is observed that the force required for deforming the specimen increases with an increase in the rubbery modulus, as the rubber modulus is directly related to CLD. Next, the temperature in the chamber is reduced to T_{low} (30 °C) while maintaining the deformed shape ring. Here, the cooling rate was not regulated. During the cooling, the transition from rubbery to glassy state and thermal contraction occurs, resulting in an increased load level to store the deformed oval shape. The force-temperature response during cooling (step 2, B–C) is shown in Figure 7(b). After cooling, the nut is rotated in the opposite direction to unload the stored oval shaped specimen (step 3, C–D). The deformed ring is taken out from the chamber and the oval shape is retained as long as the temperature is maintained below the glass transition temperature. In the experiments, all of the rings are not precisely deformed to a specific value due to manual

operation. Instead, measurement was done before and after deformation. Finally, the oval specimen is placed inside the thermal chamber without any constraint and the chamber temperature is increased to T_{high} at a rate of 3 °C/min (step 4, D–A). The laser extensometer is placed in front of open slot in the temperature chamber to measure the recoverable deflection. The free recovery of major principal axis diameter for all ratios during heating is shown in Figure 7(c). For force recovery experiments, the unloaded deformed ring is constrained and reheated to T_{high} at a rate of 3 °C/min. Initially, the SMP ring experiences a low compressive force which shoots up to reach the pre-deformation load level at their respective glass transition temperature as shown in Figure 7(d) (step 4, D–B).

The shape fixity and shape recovery ratio is calculated for all epoxy ratios compared in Table 2 as given by Liu et al. (2007). Epoxy85, the lowest hardener content have relatively higher shape fixity ratio compared with other compositions. Also epoxy85 shows the fastest recovery among the three SMPs but lower shape recovery ratio of about 84%. The epoxy85 has low CLD, low T_g and high tanδ peak. As their chain segments are less constrained in the permanent network favours high chain mobility for easy deformation and quicker shape recovery. This shows that the CLD has an influence on shape fixing ratio and shape recovery speed. Among all of the ratios, epoxy100 shows higher shape recovery ratio of 96%. The epoxy115 SMP with excess hardener content, shows faster recovery than epoxy100 and also lower shape recovery ratio (91%) than epoxy100. In the DMA, the tanδ curve also depicts this behaviour. The lower transition bandwidth in epoxy115 shows that the material is slightly sensitive than epoxy100. This may be due to the less homogenous chain segments between the networks due to excess hardener content.

Shape memory cycle for various deformation levels

The epoxy85 and epoxy100 rings are subjected to various deflections during the shape memory cycle experiments. The epoxy85 ring is loaded at $T_g + 12$ °C for 10 mm ($D_f = 70$ mm) and 15 mm ($D_f = 75$ mm) diametric deflections. However, for 20 mm ($D_f = 80$ mm) deflection, the ring is loaded at $T_g + 8$ °C to avoid breakage near the hooks. The load response during the shape memory cycle (ABCD) for various deflections in epoxy85 is shown in Figure 8(a). It is observed that loading near T_g for 20 mm takes a higher load to deform, as the modulus increases. The free shape recovery profile for various diametric deflections is shown in Figure 8(b). For lower deflection ($D_f = 70$ mm) low shape recovery is observed than higher deflections ($D_f = 75$ mm, 80 mm). The same epoxy85 rings are again subjected to a second set of shape ($A_2B_2C_2D_2$) memory cycle tests with similar values of deflections as
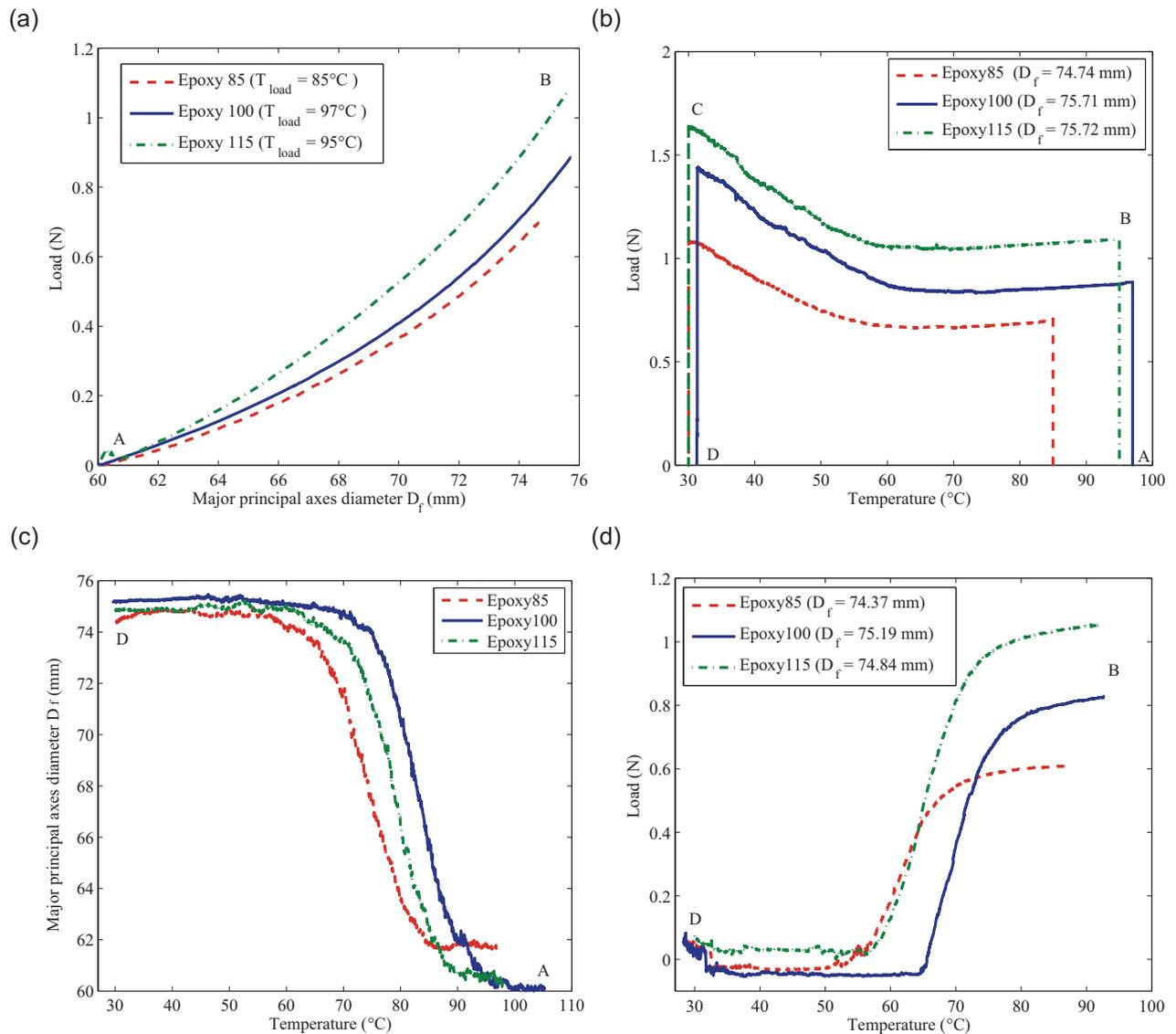
(a)

(b)

(c)

(d)

Figure 7. Shape memory cycle for different epoxy ratios.

Table 2. Shape fixity and recovery ratio for different epoxy ratios.

Epoxy ratios	Shape fixity (%)	Shape recovery (%)
Epoxy85	97.4	84.4
Epoxy100	96.62	95.86
Epoxy115	94.4	91

the first set. For the second cycle, the shape recovery increases for all the deflections. The two consecutive shape memory cycles for 15 mm deflection (D_f = 75 mm) is shown in Figure 9. The shape recovery increases from 84% in the first cycle to 94% in the second cycle. A near complete shape recovery is possible by training the material but the accumulation of irrecovery shape during the initial cycles will remain.

In epoxy85, plastic deformation occurs as the chain segments are loosely restricted by the networks results in the accumulation of the irrecoverable shape.

Similarly, the shape memory cycle for various deflections in epoxy100 is carried out. The isothermal loading curve of epoxy100 is shown in Figure 10(a). For 10 and 15 mm deflections, the rings are loaded at T_g + 12 °C. However, for 20 mm deflection, the ring is loaded at T_g, as it requires less load for deformation due to high viscous nature at tanδ peak. For 25 mm deflection, the specimen was loaded at T_g − 2 °C. In the current section, shape recovery profile is focussed for various deflections. The effects of various loading temperatures on SMPs will be discussed in the following sections. It is noted that all of the specimens are loaded between the T_{high} or near to T_g peak. The load–temperature response for epoxy100 SMPs is shown in Figure 10(b) and free shape recovery graph is presented
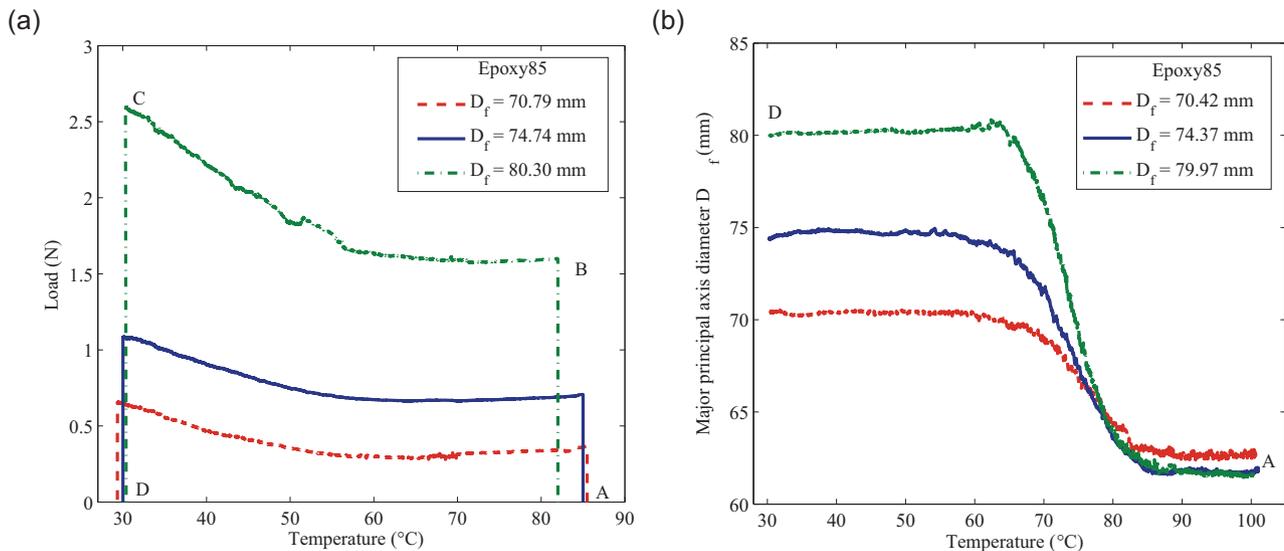
(a)

(b)

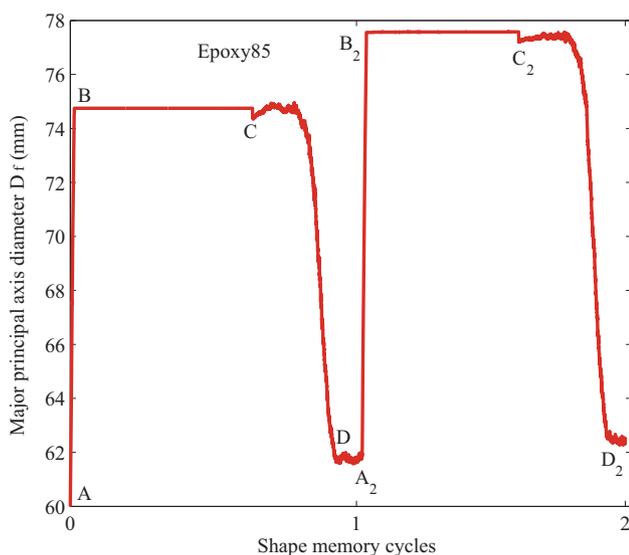**Figure 8.** Shape memory cycle for various deflection in epoxy85.

Figure 9. Two subsequent cycles in epoxy85: ABCD and $A_2B_2C_2D_2$.

in Figure 10(c) with 96% of shape recovery for all deflections.

Memory characteristics

In the current section, the memory characteristics for epoxy100 SMPs are studied based on different loading and unloading temperatures. In the first case, the shape memory cycle is performed at different loading temperatures (T_{load}) in the transition region such as 97 °C, 86 °C, 75 °C and 65 °C. The loading curve to deform the ring (D_f = 75 mm) at different temperatures is shown in Figure 11(a). Loading at temperatures 95 °C and 86 °C, shows non-linear behaviour. Loading at

86 °C (T_g) takes less load than loading at 97 °C. At T_g, the polymer chains undergo rapid vibrational movements and increased chain flexibility. So the stress relaxation occurs immediately at time of loading and hence it takes less load to deform at T_g. Loading at temperatures below T_g (65 °C and 75 °C) shows nearly linear behaviour as the stiffness increases. The load–temperature response for loading at different temperatures in the shape memory cycle is shown in Figure 11(b). The ring loaded at 75 °C and 65 °C shows a sudden decrease in the load immediately after loading process and then slightly increases during cooling. At below T_g, polymer chains takes more time to relax the stresses. Here cooling was carried out without giving much time for relaxation, so the sudden drop in load is noticed over a small temperature range. The memory storage below T_g is due to entropy and as well as internal energy. The shape fixity ratio of 96–97% is observed for all of these loading temperatures. The shape recovery curve for loading at various temperatures is shown in Figure 11(c). It is observed that there is slight shift in shape recovery curve around 3–4 °C when loaded above and below T_g. The shape recovery ratio above T_g is 96% and decreases to 93% when loaded below T_g.

In the second case, all of the rings are deformed (D_f = 75 mm) at 97 °C and unloaded at 85 °C and 60 °C as shown in the load–temperature response curve in Figure 12(a). During cooling, the deformed shape is transformed from a rubbery to a glassy state. The shape storage is a temperature-dependent process. The shape fixity also depends on the unloading temperature. When loaded at T_g or above, it is observed that most of the shape is released due to entropy. When unloaded at 85 °C, 10% of deformed shape remains fixed and 96% of shape fixity at 60 °C is observed,
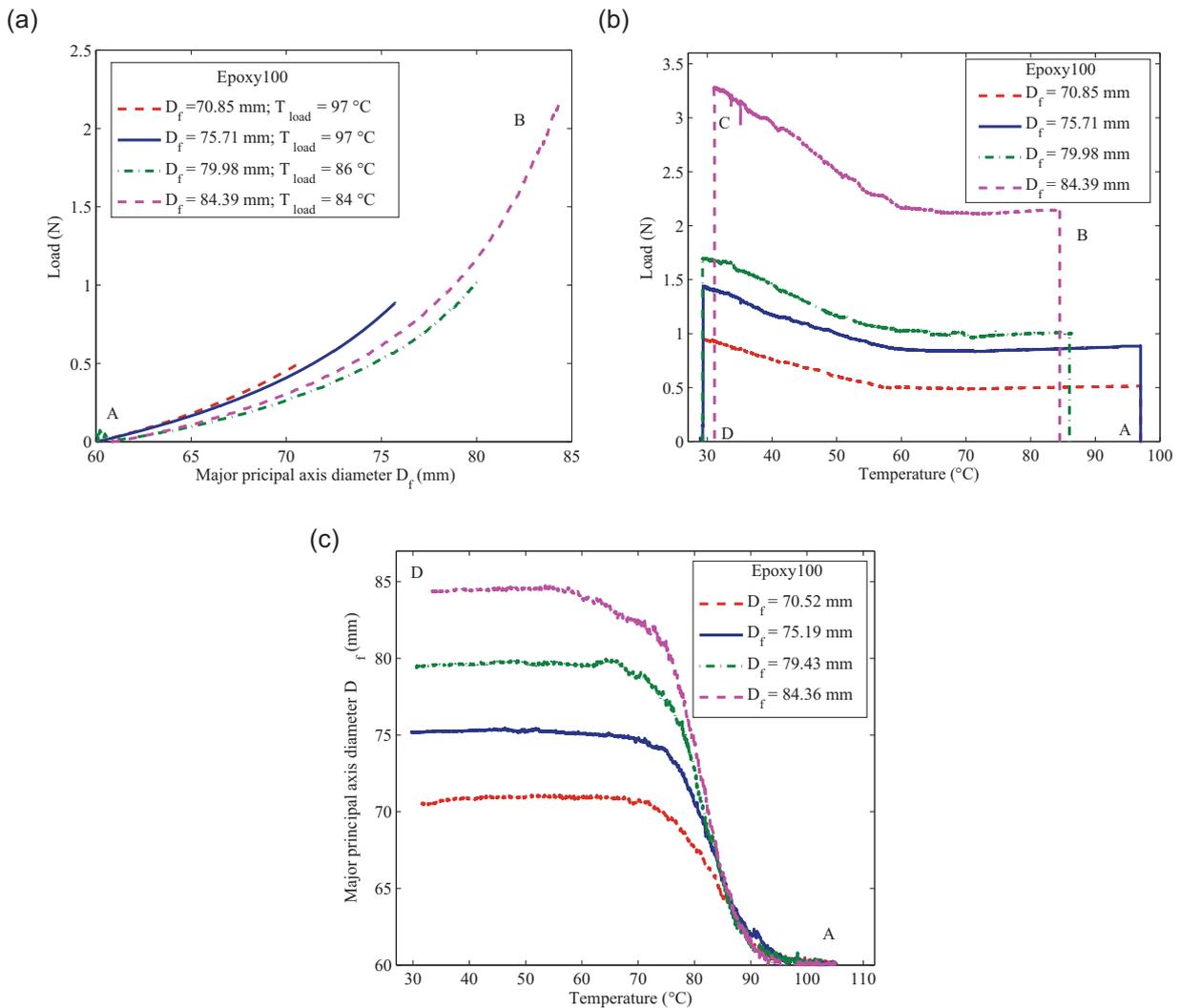
Figure 10. Shape memory cycle for various deflection in epoxy100.

similar to unloading at 30 °C. The shape recovery curve is shown in Figure 12(b). For 85 °C and 60 °C unloading, about 1% loss of shape recovery is observed. The loading and the unloading temperature also influences the shape fixity and shape recovery ratio.

Numerical simulations

Numerical simulation of this ring is carried out using a small deformation model implemented in ABAQUS-VUMAT proposed by the authors based on theory of multiple natural configurations. This framework focuses on modelling the two unique features of SMP such as temperature- and deformation-dependent change in stiffness and shape memory characteristics. This model is primarily rate-independent thermo-elastic neglecting viscous effects but all these features can be accommodated in the model. A small deformation model is implemented and correlated with existing

experiments in the literature (Sujithra et al., 2014). The stress-free configuration is known as a natural configuration. The SMP body will undergo changes in natural configuration during cooling/heating, as it passes through the T_g. Such a body is said to possess multiple natural configurations (Rajagopal and Srinivasa, 2004). The shape memory characteristics are modelled by assuming the reversible transformation between reference and natural configuration depending upon the temperature and current deformed state. Based on the DMA curve, the natural configuration is tracked using a suitable temperature-dependent parameter called the degree of glass transition parameter (dogt), which also describes the loading and unloading process from this natural configuration. The transition from one natural configuration to the other takes place upon changing this parameter. All material property changes are associated with this parameter that represents the change in natural configuration. Here storing and releasing processes are strictly reversible.
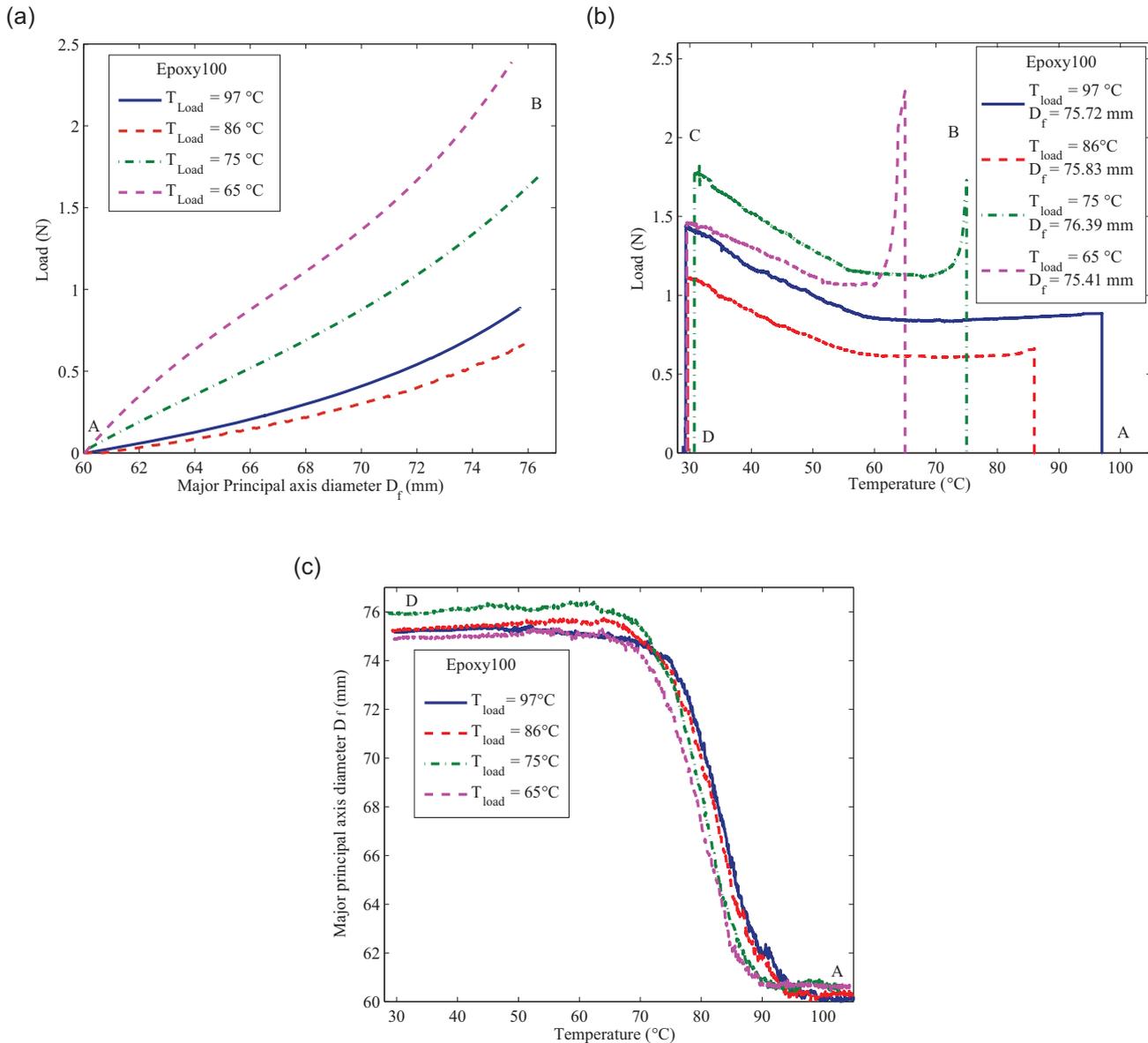
Figure 11. SMP cycle for epoxy100 at different loading temperatures.

The shape memory cycle for epoxy100 is simulated using a finite element model of the half SMP ring and rigid plate with boundary conditions, shown in Figure 13. Frictionless contact is defined between ring surface and rigid plate. The SMP ring is discretized into 60 elements and C3D8RT (coupled temperature–displacement) element is chosen in ABAQUS explicit. The most striking feature of the explicit method is the absence of a global tangent stiffness matrix, which is required with implicit methods. Since the state of the model is advanced explicitly, iterations and tolerances are not required. The material parameters for this simulation are obtained from characterization results, given in Table 3. From the DMA curve (epoxy100), the glass transition temperature is found to be 86 °C and the

temperature range is chosen from 30 °C (T_{low}) to 97 °C (T_{high}). The modulus fit curve for epoxy100 is shown in Figure 14. In this simulation, the glassy thermal expansion coefficient is considered to be constant during the entire cycle. Initially, the ring is subjected to a pre-defined temperature at 97 °C and the plate is moved in vertical direction (2-axis) to stretch the ring (A–B). The plate is maintained in the same position, as the temperature reduces from 97 °C to 30 °C (B–C). After cooling, the contact between the SMP ring and rigid plate is deactivated and the plate moves back to the initial position (C–D). The unloaded ring is reheated to 97 °C (D–A), the deformed ring regain its permanent shape. In force recovery simulations after unloading, the deformed ring is constrained and reheated (D–B).
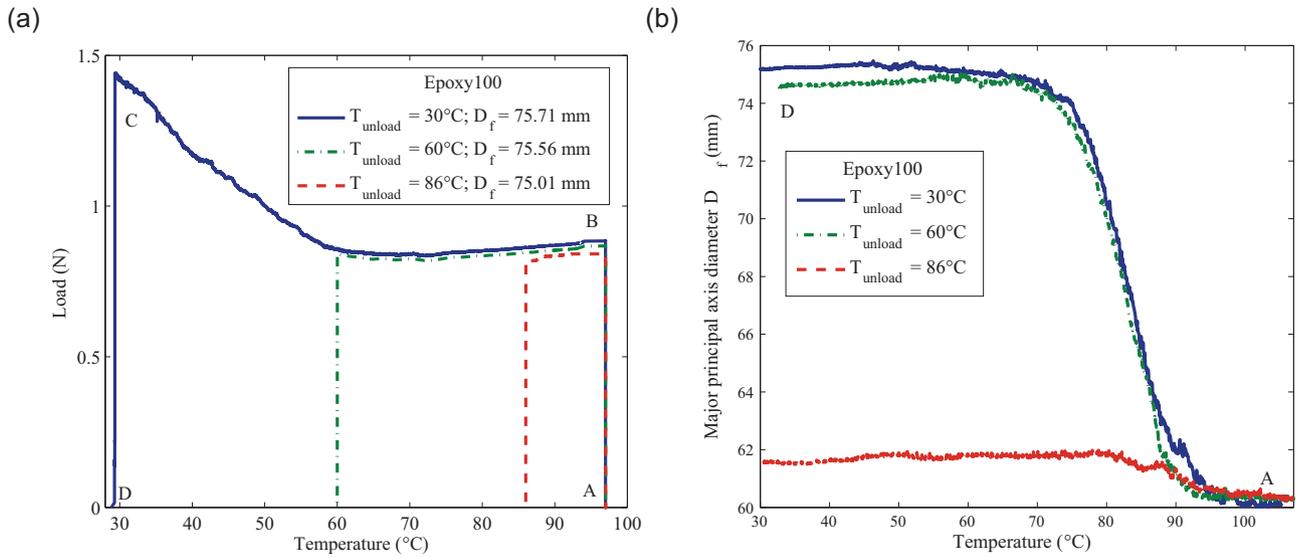
(a)

(b)

Figure 12. SMP cycle for epoxy100 at different unloading temperatures.
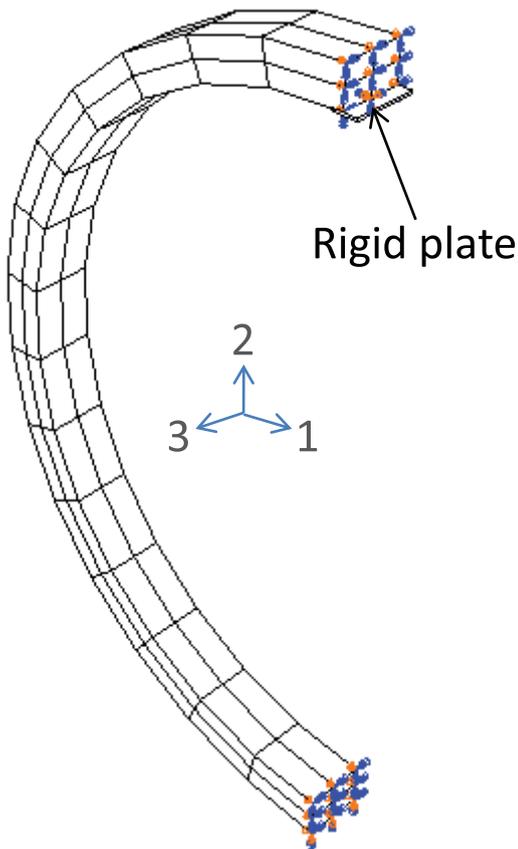

Figure 13. Finite element model of symmetric ring and plate with boundary conditions.

The experiment results for various deflections in epoxy100 are compared with simulation results are discussed here. The load–temperature response is shown in Figure 15(a). For an increase in deflections levels,

Table 3. Material constants for numerical simulation.

Material constants	Values
Rubbery modulus	23.16 (MPa)
Glassy modulus	2300 (MPa)
Bulk modulus	1000 (MPa)
Poisson's ratio (rubbery state)	0.49
Poisson's ratio (glassy state)	0.4
Coefficient of thermal expansion	0.48×10^{-4} (1/°C)
Cross-link density	2.492×10^{-3} (mol/cm³)
Coefficient of dogt parameter	
a	2.7×10^{-5} (1/°C⁴)
n	4.25

dogt: degree of glass transition parameter.
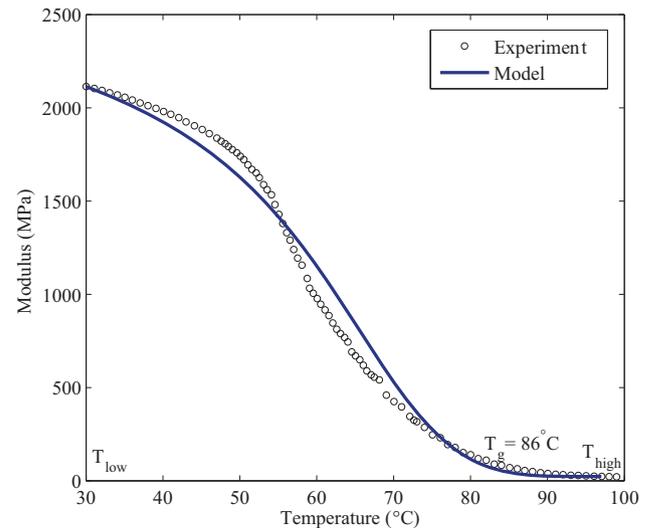

Figure 14. Variation of modulus with temperature.
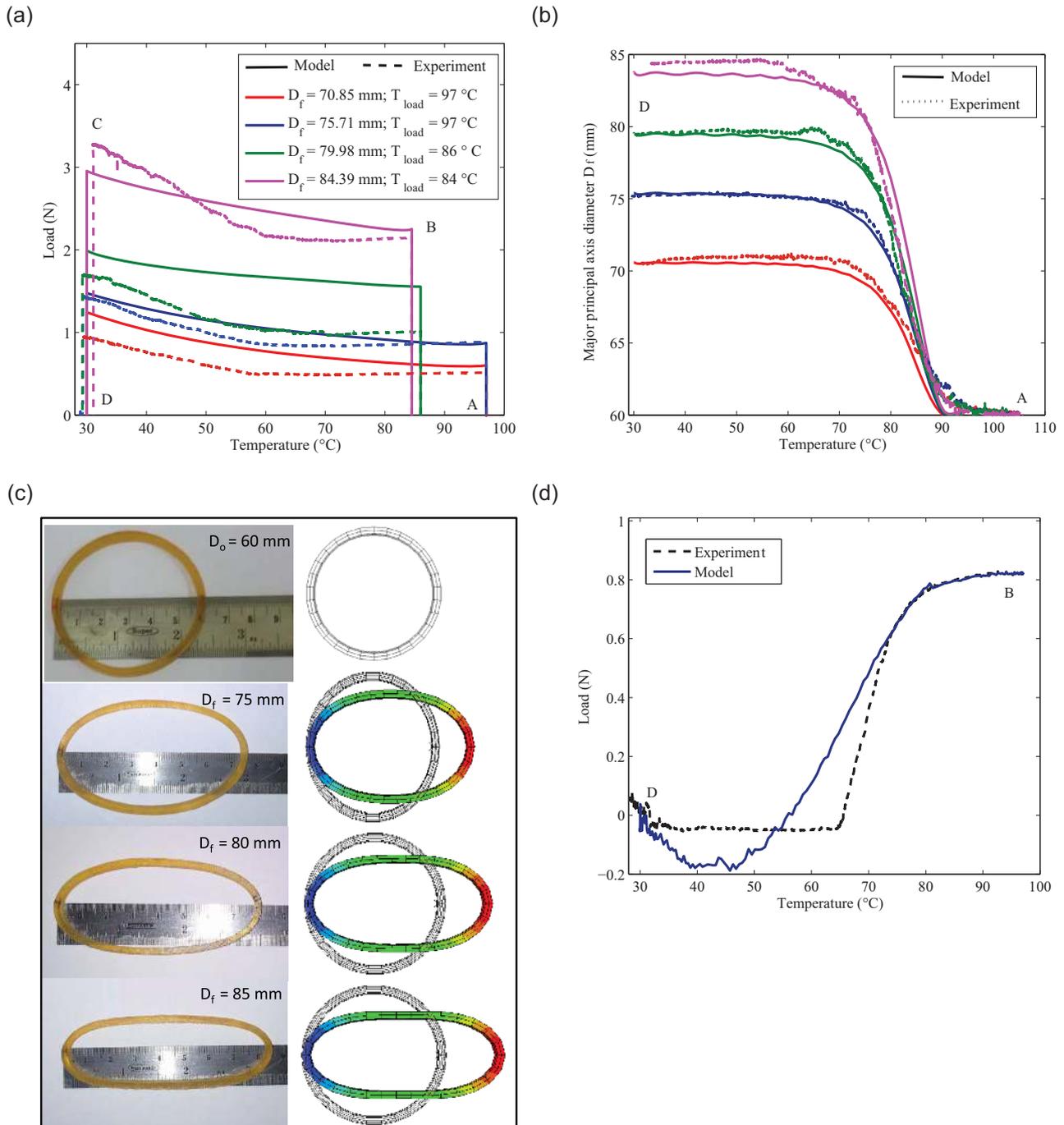
(a)

(b)

(c)

(d)

Figure 15. Shape memory cycle experiments and numerical simulation for epoxy100.

the simulation shows increased load levels. The model implemented is a small strain model neglecting the viscous effect. But in the experiments, it shows non-linear behaviour during loading and the rate of cooling process is non-uniform. The simulation results for loading at T_g is not reflected in the model. The model proposed was based on thermo-mechanical history of shape storage process during cooling and it retraces the path during shape recovery. But, VUMAT stores only two-state architecture; the initial values are in old arrays and the

current values are in new arrays. So, at the end of unloading, the final amount of stored strain is stored in old array. By using this old stored array, the new stored strain is released during reheating. The shape recovery for various deflections is compared in Figure 15(b), which depicts the capability of the model to capture shape recovery for large deflections. The deformed ring sample and finite element deformed ring for various deflections is shown in Figure 15(c). The force recovery simulations for $D_f \approx 75$ mm is shown in Figure 15(d).
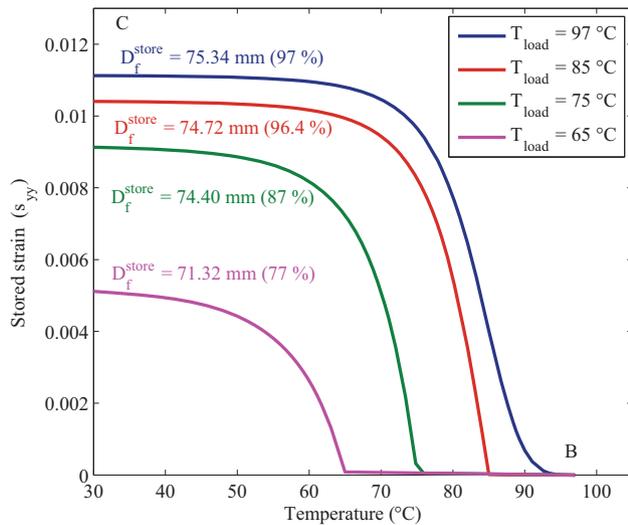
Figure 16. Simulation effect of strain storage during cooling (step 2, BC) for loading at different temperatures in epoxy100.

Figure 17. Free shape recovery for unloading at different temperatures.

Due to shape recovery constraint in the reheating simulation, the ring experiences a high compressive force below T_g and then the load shoots to the pre-deformed load level at T_g. But in the experiments, initially thermal expansion dominates which is not captured in the model due to two-state storage architecture in ABAQUS-VUMAT.

The memory characteristics study involves loading and unloading at different temperatures. Instead of shape recovery, the history of shape storage (stored strain) during cooling for loading at different temperatures is shown in Figure 16. Simulation results show that shape storage ratio drops down from 97% ($T_{load} = 97 \degree C$) to 77% ($T_{load} = 65 \degree C$) when loaded below T_g. But in the experiments, 96% (above T_g) to 93% (below T_g) of shape storage is observed for loading at different temperatures in the transition band. The shape recovery simulation result for unloading at different temperatures is shown in Figure 17. During reheating, shape recovery curve follows the same path from the unloading temperature. If unloading occurs nearer to T_g, then it is likely that the experiment and modelling can widely vary since there is an abrupt change in storage capacity. Because of this, the sensitivity of storage to temperature is found to be high. For unloading at 60 °C and 30 °C, the shape storage ratio is about 96–95% in both experiment and simulation.

Conclusion

Shape memory behaviour of an amorphous polymer has been studied experimentally using epoxies with different hardener ratios. A hardener ratio of epoxy that falls a little below the stoichiometric ratio for complete cross-link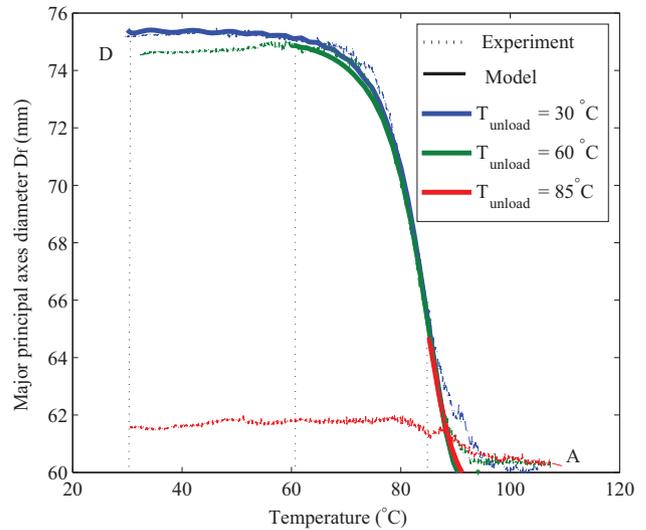ing shows a high shape fixing ratio and a narrow transition band. However, a complete cross-linking ratio is found to be necessary for high shape recovery but with a compromise on the width of the transition band. The temperature at which loading/unloading is carried out is found to be an important parameter in the memory actuation process. Irrespective of temperatures below T_g when the fixity is introduced, the recovery part of the shape memory cycle occurs only around the T_g. This is expected to be the case for the amorphous polymers. This memory characteristic study helps in modelling the behaviour and designing smart systems. To capture the true shape memory behaviour of an amorphous polymer, it is necessary to include viscous effects in the study. Future work will be focused on implementing the viscous effects in the model.

References

Atli B, Gandhi F and Karst G (2009) Thermomechanical characterization of shape memory polymers. *Journal of Intelligent Material Systems and Structures* 20: 87–95.

Behl M and Lendlein A (2007) Shape-memory polymers. *Materials Today* 10: 20–28.

Castro F, Westbrook KK, Hermiller J, Ahn DU, Ding Y and Qi HJ (2011) Time and temperature dependent recovery of epoxy-based shape memory polymers. *Journal of Engineering Materials and Technology* 133: 021025.

Chen J, Liu L, Liu Y and Leng J (2014) Thermoviscoelastic shape memory behavior for epoxy-shape memory polymer. *Smart Materials and Structures* 23: 055025.

Diani J, Fredy C, Gilormini P, Merckel Y, Regnier G and Rousseau I (2011) A torsion test for the study of the large deformation recovery of shape memory polymers. *Polymer Testing* 30: 335–341.

Fan M, Yu H, Li X, Cheng J and Zhang J (2013) Thermomechanical and shape-memory properties of epoxy-based shape-memory polymer using diglycidyl ether of ethoxylatedbisphenol-A. *Smart Materials and Structures* 22: 055034.

Garcia FG, Soares BG, Pita VJRR, Sanchez R and Rieumont J (2007) Mechanical properties of epoxy networks based on DGEBA and aliphatic amines. *Journal of Applied Polymer Science* 106: 2047–2055.

Ghosh P, Rao A and Srinivasa AR (2013) Design of multistate and smart-bias components using shape memory alloy and shape memory polymer composites. *Materials and Design* 44: 164–171.

Guo X, Liu L, Liu Y, Zhou B and Leng J (2014) Constitutive model for a stress- and thermal induced phase transition in a shape memory polymer. *Smart Materials and Structures* 23: 105019.

Hu J, Zhu Y, Huang H and Lu J (2012) Recent advances in shape-memory polymers: Structure, mechanism, functionality, modeling and applications. *Progress in Polymer Science* 37: 1720–1763.

Lan X, Liu Y, Lv H, Wang X, Leng J and Du S (2009) Fiber reinforced shape-memory polymer composite and its application in a deployable hinge. *Smart Materials and Structures* 18: 024002.

Lendlein A and Behl M (2008) Shape memory polymers for biomedical applications. *Advances in Science and Technology* 54: 96–102.

Lendlein A and Kelch S (2002) Shape-memory polymers. *Angewandte Chemie International Edition* 41: 2034–2057.

Leng J, Lan X, Liu Y and Du S (2011) Shape-memory polymers and their composites: Stimulus methods and applications. *Progress in Materials Science* 56: 1077–1135.

Leng J, Lv H, Liu Y and Du S (2007) Electroactivate shapememory polymer filled with nanocarbon particles and short carbon fibers. *Applied Physics Letters* 91: 144105.

Leonardi AB, Fasce LA, Zucchi IA, et al. (2011) Shape memory epoxies based on networks with chemical and physical crosslinks. *European Polymer Journal* 47: 362–369.

Li G (2014) *Self-Healing Composites: Shape Memory Polymer Based Structures*. Chichester: John Wiley and Sons, Inc..

Li G and Xu W (2011) Thermomechanical behavior of thermoset shape memory polymer programmed by cold-compression: testing and constitutive modeling. *Journal of the Mechanics and Physics of Solids* 59: 1231–1250.

Liu C, Qin H and Mather PT (2007) Review of progress in shape-memory polymers. *Journal of Materials Chemistry* 17: 1543–1558.

Liu Y, Du H, Liu L and Leng J (2014) Shape memory polymers composites and their applications in aerospace: a review. *Smart Materials and Structures* 23: 023001.

Liu Y, Gall K, Dunn ML, Greenberg AR and Diani J (2006) Thermomechanics of shape memory polymers: Uniaxial experiments and constitutive modelling. *International Journal of Plasticity* 22: 279–313.

Liu Y, Gall K, Dunn ML and McCluskey P (2003) Thermomechanical recovery couplings of shape memory polymers in flexure. *Smart Materials and Structures* 12: 947–954.

Liu Y, Lv H, Lan X, Leng J and Du S (2009) Review of electro-activate shape-memory polymer composite. *Composites Science and Technology* 69: 2064–2068.

Lv H, Du H, Liu L and Leng J (2008) Shape-memory polymer in response to solution. *Advanced Engineering Materials* 10: 592–595.

Maitland DJ, Metzger MF, Schumann D, Lee A and Wilson TS (2002) Photothermal properties as shape memory polymer micro-actuators for treating stroke. *Laser in Surgery and Medicine* 30: 1–11.

McClung AJW, Tandon GP and Baur JW (2013) Deformation rate, hold time, and cycle-dependent shape-memory performance of Veriflex-E resin. *Mechanics of Time-Dependent Materials* 17: 39–52.

McClung AJW, Tandon GP, Goecke KE and Baur JW (2011) Non-contact technique for characterizing full-field surface deformation of shape memory polymers at elevated and room temperatures. *Polymer Testing* 30: 140–149.

Meng H and Li G (2013) A review of stimuli-responsive shape memory polymer composites. *Polymer* 54: 2199–2221.

Mohr R, Kratz K, Weigel T, Lucka M, Moneke M and Lendlein A (2006) Initiation of shape memory effect by inductive heating of magnetic nanoparticles in thermoplastic polymers. *Proceedings of the National Academy of Sciences of the USA* 103: 3540–3545.

Rajagopal KR and Srinivasa AR (2004) On the thermomechanics of materials that have multiple natural configurations part 1: Viscoelasticity and classical plasticity. *Zeitschrift für Angewandte Mathematik und Physik (ZAMP)* 55: 861–893.

Ratna D and Kocsis JK (2008) Recent advances in shape memory polymers and composites: a review. *Journal of Material Science* 43: 254–269.

Rimdusit S, Lohwerathana M, Hemvichian K, Kasemsiri P and Dueramae I (2013) Shape memory polymers from benzoxazine-modified epoxy. *Smart Materials and Structures* 22: 075033.

Rousseau IA (2008) Challenges of shape memory polymers: a review of the progress toward overcoming SMP's limitations. *Polymer Engineering and Science* 48: 2075–2089.

Rousseau IA and Xie T (2010) shape memory epoxy: composition, structure, properties and shape memory performances. *Journal of Materials Chemistry* 20: 3431–3441.

Schmidt C, Neuking K and Eggeler G (2008) Functional fatigue of shape memory polymers. *Advanced Engineering Materials* 10: 922–927.

Sekkar V, Narayanaswamy K, Scariah KJ, Nair PR, Sastri KS and Ang HG (2007) Evaluation by various experimental approaches of the crosslink density of urethane networks based on hydroxyl-terminated polybutadiene. *Journal of Applied Polymer Science* 103: 3129–3133.

Sujithra R, Srinivasan SM and Arockiarajan A (2014) Modelling memory effects in amorphous polymer. *International Journal of Engineering Sciences* 84: 95–112.

Tandom GP, Goecke K, Cable K and Baur J (2009) Durability assessment of styrene- and epoxy-based shape-memory polymer resins. *Journal of Intelligent Material Systems and Structures* 20: 2127–2143.

Volk BL, Lagoudas DC, Chen YC and Whitley KS (2010) Analysis of the finite deformation response of shape memory polymers: I. Thermomechanical characterization. *Smart Materials and Structures* 19: 075005.

Xie T (2010) Tunable polymer multi-shape memory effect. *Nature* 464: 267–270.

Xie T and Rousseau IA (2009) Facile tailoring of thermal transition temperatures of epoxy shape memory polymers. *Polymer* 50: 1852–1856.

Yakacki CM, shandas R, lanning C, Rech B, Eckstein A and Gall K (2007) Unconstrained recovery characterization of shape-memory polymer networks for cardiovascular applications. *Biomaterials* 28: 2255–2263.

Zhou B, Wu X, Liu Y and Leng J (2011) Study on shape recovery behaviors of epoxy-based shape memory polymer. *Advanced Materials Research* 179–180: 325–328.

Zotzmann J, Behl M, Feng Y and Lendlein A (2010) Copolymer networks based on poly(ω-pentadecalactone) and poly(ε-caprolactone) segments as a versatile triple-shape polymer system. *Advanced Functional Materials* 20: 3583–3594.